Author's Accepted Manuscript

Cytosolic calcium mediates RIP1/RIP3 complex-dependent necroptosis through JNK activation and mitochondrial ROS production in human colon cancer cells

Wen Sun, Xiaxia Wu, Hongwei Gao, Jie Yu, Wenwen Zhao, Jin-Jian Lu, Jinhua Wang, Guanhua Du, Xiuping Chen
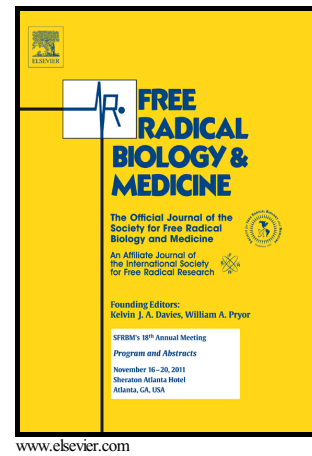
FREE RADICAL BIOLOGY & MEDICINE

The Official Journal of the Society for Free Radical Biology and Medicine
An Affiliate Journal of the International Society for Free Radical Research

Founding Editors:
Kelvin J. A. Davies, William A. Pryor

SFRBM's 18th Annual Meeting
Program and Abstracts
November 16–20, 2011
Sheraton Atlanta Hotel
Atlanta, GA, USA

www.elsevier.com

Cite this article as: Wen Sun, Xiaxia Wu, Hongwei Gao, Jie Yu, Wenwen Zhao, Jin-Jian Lu, Jinhua Wang, Guanhua Du and Xiuping Chen, Cytosolic calcium mediates RIP1/RIP3 complex-dependent necroptosis through JNK activation and mitochondrial ROS production in human colon cancer cells, *Free Radical Biology and Medicine,* http://dx.doi.org/10.1016/j.freeradbiomed.2017.04.010

Cytosolic calcium mediates RIP1/RIP3 complex-dependent necroptosis through JNK activation and mitochondrial ROS production in human colon cancer cells

Wen Sun[1], Xiaxia Wu[1], Hongwei Gao[1], Jie Yu[1], Wenwen Zhao[1], Jin-Jian Lu[1], Jinhua Wang[2], Guanhua Du[2], Xiuping Chen[1*]

[1]State Key Laboratory of Quality Research in Chinese Medicine, Institute of Chinese Medical Sciences, University of Macau, Macau, China

[2]The State Key Laboratory of Bioactive Substance and Function of Natural Medicines, Beijing Key Laboratory of Drug Target Research and Drug Screen, Institute of Materia Medica, Chinese Academy of Medical Science and Peking Union Medical College, Beijing, 100050, China.

[*]Correspondence to: Institute of Chinese Medical Sciences, University of Macau, Avenida da Universidade, Taipa, Macau, China. Tel.: +853 88224679; fax: +853 28841358. xpchen@umac.mo

ABSTRACT

Necroptosis is a form of programmed necrosis mediated by signaling complexes with receptor-interacting protein 1 (RIP1) and RIP3 kinases as the main mediators. However, the underlying execution pathways of this phenomenon have yet to be elucidated in detail. In this study, a RIP1/RIP3 complex was formed in 2-methoxy-6-acetyl-7-methyljuglone (MAM)-treated HCT116 and HT29 colon cancer cells. With this formation, mitochondrial reactive oxygen species (ROS) levels

increased, mitochondrial depolarization occurred, and ATP concentrations decreased. This process was identified as necroptosis. This finding was confirmed by experiments showing that MAM-induced cell death was attenuated by the pharmacological or genetic blockage of necroptosis signaling, including RIP1 inhibitor necrostatin-1s (Nec-1s) and siRNA-mediated gene silencing of RIP1 and RIP3, but was unaffected by caspase inhibitor z-vad-fmk or necrosis inhibitor 2-(1H-Indol-3-yl)-3-pentylamino-maleimide (IM54). Transmission electron microscopy (TEM) analysis further revealed the ultrastructural features of MAM-induced necroptosis. MAM-induced RIP1/RIP3 complex triggered necroptosis through cytosolic calcium (Ca^{2+}) accumulation and sustained c-Jun N-terminal kinase (JNK) activation. Both calcium chelator BAPTA-AM and JNK inhibitor SP600125 could attenuate necroptotic features, including mitochondrial ROS elevation, mitochondrial depolarization, and ATP depletion. 2-thenoyltrifluoroacetone (TTFA), which is a mitochondrial complex II inhibitor, was found to effectively reverse both MAM induced mitochondrial ROS generation and cell death, indicating the complex II was the ROS-producing site. The essential role of mitochondrial ROS was confirmed by the protective effect of overexpression of manganese superoxide dismutase (MnSOD). MAM-induced necroptosis was independent of TNFα, p53, MLKL, and lysosomal membrane permeabilization. In summary, our study demonstrated that RIP1/RIP3 complex-triggered cytosolic calcium accumulation is a critical mediator in MAM-induced necroptosis through sustained JNK activation and mitochondrial ROS production. Our study also provided new insights into the

molecular regulation of necroptosis in human colon cancer cells.

Abbreviations

AO, acridine orange; ATP, adenosine triphosphate; CaMK, calcium-calmodulin kinase;

EGTA, ethylenebis(oxyethylenenitrilo)tetraacetic acid; IM-54,

2-(1H-Indol-3-yl)-3-pentylamino-maleimide; JC-1,

5,5′,6,6′-tetrachloro-1,1′,3,3′-tetraethylbenzimidazolylcarbocyanine iodide; JNK,

c-Jun-N-terminal kinase; LMP, lysosome membrane permeabilization; MAM,

2-methoxy-6-acetyl-7-methyljuglone; MLKL, mixed lineage kinase domain-like;

MMP, mitochondria membrane potential; MPT, mitochondrial permeability transition;

MTS,3-(4,5-dimethylthiazol-2-yl)-5-(3-carboxymethoxyphenyl)-2-(4-sulfophenyl)-2

H-tetrazolium, inner salt; Nec-1s, necrotatin-1s; NO, nitric oxide; NSA,

necrosulfonamide; PMSF, phenylmethylsulfonyl fluoride; RIP, receptor-interacting

protein; ROS, reactive oxygen species; TEM, transmission electron microscopy;

z-vad-fmk, N-benzyloxycarbonyl-Val-Ala-Asp-fluoromethylketone

Keywords

Necroptosis; c-Jun N-terminal kinase; calcium; ROS

Introduction

Necroptosis represents a form of regulated necrosis classically initiated by death

receptors, such as tumor necrosis factor receptor 1 [1]. Identified by Degterev et al.

[2], this form of cell death involves the kinase activity of receptor-interacting protein

1 (RIP1) and RIP3, which leads to the formation of a complex termed necrosome [3]. Necrosome formation results in RIP3 activation. Activated human RIP3 is phosphorylated at Ser227, and the phosphorylated form subsequently causes the phosphorylation of human mixed lineage kinase domain-like (MLKL) protein at Thr357 and Ser358 sites. Consequently, the phosphorylated MLKL undergoes oligomerization and membrane translocation, which trigger pore formation in lipid bilayers and loss of plasma membrane integrity [4-6]. Although the initial molecular components of necroptotic pathways have been described, their downstream signaling regulatory mechanisms have remained poorly understood.

Ca^{2+} is a well-known second messenger involved in nearly every aspect of cellular life [7]. In necroptosis, Ca^{2+} influx is an important downstream event of MLKL during TNF-induced necroptosis [4]. Cytosolic calcium accumulation can trigger necroptosis by activating calcium-calmodulin kinase (CaMK) II-mediated RIP1 phosphorylation, and this phenomenon indicates that Ca^{2+} is an early upstream regulator of necroptosis [8].

The evasion of programmed cell death is considered a hallmark of cancers, and this condition can facilitate tumor initiation, progression, and drug resistance [9,10]. Necroptosis provides potential novel molecular targets and strategies for optional therapeutic intervention because of its molecular mechanism and signaling regulation distinct from those of apoptosis. The effectiveness of this strategy is temporarily indicated by shikonin, a natural naphthoquinone [11]. This substance triggers necroptotic cell death in MCF-7 and HEK293 cell lines, which can circumvent drug

resistance mediated by P-glycoprotein (P-gp), Bcl-2, and Bcl-xL [11]. Shikonin also exhibits necroptotic potency toward glioma and osteosarcoma cells [12,13]. However, its effect on necroptotic signaling remains unclear.

2-Methoxy-6-acetyl-7-methyljuglone (MAM), a natural naphthoquinone, was isolated from *Polygonum cuspidatu* [14], *Rhamnus fallax* B [15], and *Ventilago calyculata* [16] in 1983. However, its bioactivities have barely been reported [17-21]. In our previous work, MAM can induce necroptosis in A549 lung cancer cells and apoptosis in MCF7 breast cancer cells and B16-F10 melanoma cells [22]. Nitric oxide and JNK are essential mediators in this process. However, the detailed mechanisms of MAM in necroptosis remain unclear. In our study, MAM could induce human colon cancer cell death with non-apoptotic features. Basing on the formation of RIP1/RIP3 complex, the inhibitory effect of Nec-1s, and the respective phosphorylation of RIP1 and RIP3 at Ser166 and Ser227, we identified the cell death type as necroptosis. We then observed that cytosolic calcium accumulation and sustained JNK activation were the downstream events of RIP1/RIP3 complex. The blockage of calcium elevation and JNK activation attenuated the production of downstream mitochondrial reactive oxygen species (ROS), loss of mitochondria membrane potential (MMP), and depletion of ATP. On the basis of these findings, we identified a natural necroptosis inducer in human colon cancer cells for potential future applications and provided new insights into the molecular regulation of necroptosis in human colon cancer cells.

Materials and methods

Cells and reagents

Human colon cancer cell lines HCT116 p53$^{+/+}$ and HCT116 p53$^{-/-}$ cells were generous gifts of Dr. Ronggui Hu (Institute of Biochemistry and Cell Biology, Shanghai Institutes for Biological Sciences, Chinese Academy of Sciences, China). HT29 cells were purchased from Cell Bank of Type Culture Collection of Chinese Academy of Sciences (Shanghai, China). The cells were cultured in McCoy's 5A medium with 10% fetal bovine serum (Grand Island, NY, USA) and antibiotics at 37 °C in a humidified environment with 5% CO_2. We used cells within 6 months from resuscitation. MAM was isolated and purified from the dried rhizome of *P. cuspidatum* as described previously [19]. Necrosulfonamide (NSA) was from EMD Millipore Corporation (Darmstadt, Germany). 2-(1*H*-Indol-3-yl)-3-pentylamino-maleimide (IM-54) was from Abcam (Cambridge, MA, USA). Nec-1s was from BioVision (Milpitas, CA, USA). BAPTA-AM was from Molecular Probes (Eugene, OR). Ethylenebis(oxyethylenenitrilo)tetraacetic acid (EGTA) and SP600125 were from Sigma Aldrich (St Louis, MO, USA). Cathepsin inhibitor 1, E64, KN93, pepstatin A, N-benzyloxycarbonyl-Val-Ala-Asp-fluoromethylketone (Z-VAD-fmk) were from Selleckchem (Houston, TX, USA). CsA and JC-1 were from Beyotime (Shanghai, China). MitoSox Red was from Invitrogen (Carlsbad, CA, USA). Fluo-3/AM ester and tetramethylrhodamine methyl ester (TMRM) were from Molecular Probes

(Eugene, OR, USA).

Cell viability assay

Cell viability studies were performed using the CellTiter-Glo luminescent assay (Promega, Madison, WI, USA) according to the manufacturer's instructions [23]. The IC_{50} values were calculated by nonlinear regression analysis using GraphPad Prism software (San Diego, CA). Cell viability was also evaluated by CellTiter 96 AQueous One Solution Cell Proliferation Assay (Promega) kit containing the tetrazolium compound,

[3-(4,5-dimethylthiazol-2-yl)-5-(3-carboxymethoxyphenyl)-2-(4-sulfophenyl)-2*H*-tetr azolium, inner salt; MTS] according to the manufacturer's protocols. The absorbance at 490 nm with a microplate reader (FlexStation 3 microplate reader; Molecular Devices, Sunnyvale, CA) is recorded.

Western blot analysis

Preparation of cell lysates, determination of protein concentrations, electrophoresis, and immunoblotting were conducted as described previously [22]. The following antibodies were obtained from Cell Signaling Technology (Beverly, MA, USA): caspase 3 (9665S), caspase 8 (9746s), caspase 9 (9502s), GAPDH (5174S), JNK (9252S), MLKL (14993S), pCaMKII (12716S), pJNK (4668S), pRIP1 (65746S), RIP1 (3493S), RIP3 (13526S), horseradish peroxidase-conjugated secondary antibodies (7074V). pMLKL(ab187091) and pRIP3(ab209384) were from Abcam

(Cambridge, UK). Chemiluminescence signals were collected and analyzed using a ChemiDoc™ MP Imaging System with Image Lab 5.1 software (Bio-Rad, Hercules, CA, USA).

Transfections

For siRNA knockdown, cells were transfected with indicated siRNAs using Lipofectamine 3000 (Invitrogen, Carlsbad, CA, USA) according to the manufacturer's protocols and assayed 48 h after transfection. The siRNA sequences are as follow (5′-3′): RIP1 target sequence, AUCAAUCUGAGACUGUGUGAAGCCCdTdT; RIP3 target sequence, GCAGUUGUAUAUGUUAACGAGCGGUCGdTdT; MLKL target sequence, CAAACUUCCUGGUAACUCAdTdT; JNK1 target sequence, GACCUAAAUAUGCUGGAUAdTdT; JNK2 target sequence, GGAAGAAAGAAGCAAGAAUdTdT.

Co-immunoprecipitation

Cells were resuspended in IP Lysis Buffer (Pierce, Rockford, IL, USA) containing 1% PMSF and 1% protease inhibitor cocktail on ice for 15 min. After centrifugation, the obtained supernatant was mixed with 40 μL protein A/G–agarose beads (Santa Cruz, CA, USA) and 5 μL primary antibody against RIP3 overnight at 4 °C. Immunoprecipitated protein was washed for at least six times with IP Lysis Buffer, then boiled in SDS sample buffer for further immunoblotting assays.

MitoSox Red staining

MitoSox Red was employed to analyze the mitochondrial superoxide anion generation. At the end of MAM incubation with or without inhibitors pretreatment for the indicated time point, MitoSox Red (5 μM) was added to the culture medium and stained for 30 min at 37 °C, followed by signal collection by a FACSCanto flow cytometer (Becton-Dickinson, Oxford, UK).

Measurement of MMP

For the measurement of MMP, TMRM (100 nM) was applied after MAM insult to cultures with and without inhibitor pretreatment for the indicated time point. The TMRM signal was analyzed by flow cytometry. 5,5′,6,6′-tetrachloro-1,1′,3,3′-tetraethylbenzimidazolylcarbocyanine iodide (JC-1, 2 μg/mL, 30 min, 37 °C) was also used to monitor the MMP with IN Cell Analyzer 2000 (GE Healthcare, Little Chalfont, Buckinghamshire, UK). The results obtained from flow cytometer were analyzed using FlowJo software (TreeStar, San Carlos, CA, USA).

Aconitase activity

Cytosolic aconitase activity was monitored with a colorimetric assay kit (K716-100; BioVision Incorporated, Mountain View, CA, USA) according to the manufacturer's instructions. For cytosolic aconitase assay, 10^6 cells were homogenized on ice in 0.1 mL cold assay buffer, followed by centrifugation at 800 g for 10 minutes at 4 ° C. The supernatant was collected and considered as cytosolic lysates. For the mitochondrial part, the supernatant was centrifuged at 20, 000 g for 15 minutes at

4 °C, then dissolve the pellet into 0.1 mL cold assay buffer followed by sonication for 20 seconds.

Measurement of calcium by Fluo-3/AM ester and GcAMP3

For the measurement of calcium, cells were incubated with Fluo-3/AM ester (5 μM, 30 min, 37 °C) after MAM challenge with and without inhibitor pretreatment. To further confirm the involvement of calcium, cells were transfected with the GcaMP3 plasmid DNA (2.5 μg) using 5 μL Lipofectamine 3000. After transfection for 24 h, cells were treated with MAM for various time points. Images were taken using a confocal laser scanning microscopy (Leica, SP8, Germany).

Measurement of LMP

Lysotracker red (Beyotime, Shanghai, China) was used to monitor the functional state of lysosome. After MAM treatment for different time points, lysotracker red (50 nM) was incubated for another 1 h at 37 °C, followed by flow cytometry analysis. Acridine orange (AO) was another probe applied to determine the LMP. After cells were treated with MAM, AO (10 μg/mL) was added to culture medium and incubated for 15 min at 37 °C before image acquisition by IN Cell Analyzer 2000.

Apoptosis assay

Apoptosis assay was determined by PE Annexin V Apoptosis Detection Kit I (BD Pharmingen, San Diego, CA, USA) according to the manufacturer's instructions. Caspase activities was assayed with the Caspase-Glo Assay Kit (Promega, Madison,

WI, USA) as our previous report [22].

Overexpression of manganese superoxide dismutase (MnSOD) in HCT116 cells

The HCT116 cells were transiently transfected with pMnSOD plasmid (Origene, USA) tagged with Myc-DDK at the C-terminal or an empty vector using lipofectamine 3000 (Life Technologies, USA) according to the manufacture's protocol.

Enzyme-linked immunosorbent assay for detection of TNFα

Cells were seeded onto 12-well plates. The next day, MAM suspended in culture medium (1 mL) was added for the indicated time points. Enzyme-linked immunosorbent assay (ELISA) assay was performed using a commercial ELISA kit (EHC103a, eBioscience, Shenzhen, China) according to the manufacturer's instructions.

Monitoring necroptosis by high-resolution time-lapse imaging

HCT116 cells were loaded with fluorescent probes (TMRM, 100 nM; SYTOX Green, 1 μM; Hoechst 33258, 5 μg/mL) for 30 min before treatment with MAM (10 μM). Cells were imaged using a Leica SP8 laser scanning confocal microscope (Leica, Wetzlar, Germany) equipped with a HC PL APOCS2 63×x/1.40 oil objective (Leica, Wetzlar, Germany). Three-dimensional live-cell imaging (x, y, z and t) was performed in differential interference contrast and multiple fluorescence modes. For each imaging event, z sections had a total depth of 11 μm with a step size of 1 μm. The processing of images was performed using ImageJ software.

TEM assay

After MAM treatment for 8 h, cells were harvested and washed in 0.1 M PBS, centrifuged at 1,500 rpm, and then immediately fixed with 1.6 % glutaraldehyde for 1 h at 4 ℃. After fixing again in aqueous 2% osmium tetroxide, cells were dehydrated in graded series of ethanol and embedded in Epon. Ultra-thin sections were cut and stained with uranyl acetate and lead citrate. The samples were examined under a transmission electron microscope (H-7650, Hitachi, Japan) at 80 kV.

Statistical analysis

Two-sided Student's *t*-test was used to compare differences between two groups. One-way analysis of variance (ANOVA) followed by Dunnett's *post hoc* test or two-way ANOVA followed by Bonferroni *post hoc* test was used to compare differences more than two groups. A *P* value of less than 0.05 was considered statistically significant.

Results

MAM induces non-apoptotic cell death

The *in vitro* potency of MAM on colon cancer cell lines was determined by measuring the cellular ATP levels. As shown in Fig. 1, the ATP levels in both HCT116 and HT29 cells decreased dramatically in a concentration-dependent manner in response to MAM. The cellular ATP levels of both HCT116 and HT29 cells dropped rapidly to the minimum as early as 8 h. IC_{50} of MAM for HCT116 and HT29 cells were 5.2 and 7.5 μM, respectively. We then examined if MAM induced apoptosis.

Hoechst 33258 was used to label nuclear DNA in living cells (Supplementary Video 1). No chromatin condensation, one of the essential characteristics of apoptosis, was found. Instead, the cells showed signs of necrotic cell death morphology, with the loss of plasma membrane integrity as evidenced by the increased SYTOX Green fluorescence (Supplementary Video 1).
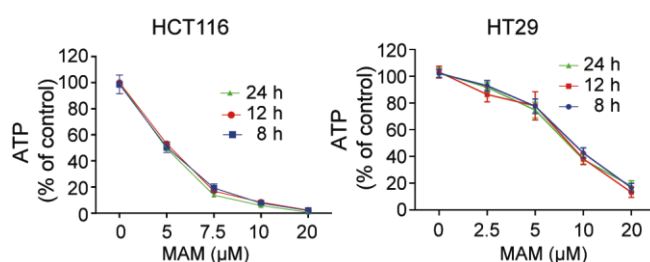
Fig. 1. MAM caused ATP depletion in colon cancer cells. Dose- and time-response analysis of MAM treatment on HCT116 and HT29 cells. Cells were treated with different concentrations of MAM for 8, 12, and 24 h, the ATP levels were determined using the CellTiter-Glo ATP-based luminescence assay. Error bars represent standard deviations of three separate experiments.

MAM-induced cell death in both HCT116 and HT29 cells neither involved externalization of phosphatidyl-serine on the cell membrane (Fig. 2A, B), a signal for early apoptosis, nor could be attenuated by z-vad-fmk (Fig. 2C, D), a pan-caspase inhibitor. After treatment with 10 and 20 μM MAM for 6 h, the necrotic (Annexin V−/PI+) rates of HT29 cells were 9.97% and 29.4%, and late apoptotic (Annexin V+/PI+) rates were 13.1% and 13.6%, respectively. In contrast, no obvious elevation of early apoptotic (Annexin V+/PI−) rates were observed. Similar results were found in HCT116 cells. The rate of late apoptosis could be significantly decreased by

Nec-1s, indicating that MAM induced necroptotic cell death in colon cancer cells. To exclude the role of apoptosis in MAM-induced colon cancer death, we examined the activities of caspases 3/7, -8, and -9. MAM treatment for 8 h did not evidently affect caspase 3/7 activities in HCT116 cells (Fig. 2E). On the contrary, the basal caspase 3/7 activities in HT29 cells were reduced to 70% of the control group (Fig. 2F). Notably, both cell lines exhibited a severe decrease in basal caspase 8 and 9 activities after MAM treatment. Furthermore, no cleavage of caspases 3, 8, and 9 was detected by Western blot analysis (Fig. 2G, H). However, the expression of pro-form caspase 8 in both cell lines declined remarkably, and this finding was similar to the reduced basal caspase 8 activity. Therefore, apoptosis was not responsible for MAM-induced cell death in HCT116 and HT29 cells. This is further confirmed by the morphological findings obtained by TEM. TEM analysis of MAM-treated cells showed no apoptotic features (Fig. 2I). Instead, the cells exhibited a typical necrotic cell death morphology, including an increasing translucent cytoplasm, swelling of organelles (especially mitochondria) with cell nuclei less affected. Along with its rapid effect on plasma membrane integrity and ATP production, we hypothesized that MAM induced necroptosis in these cells.
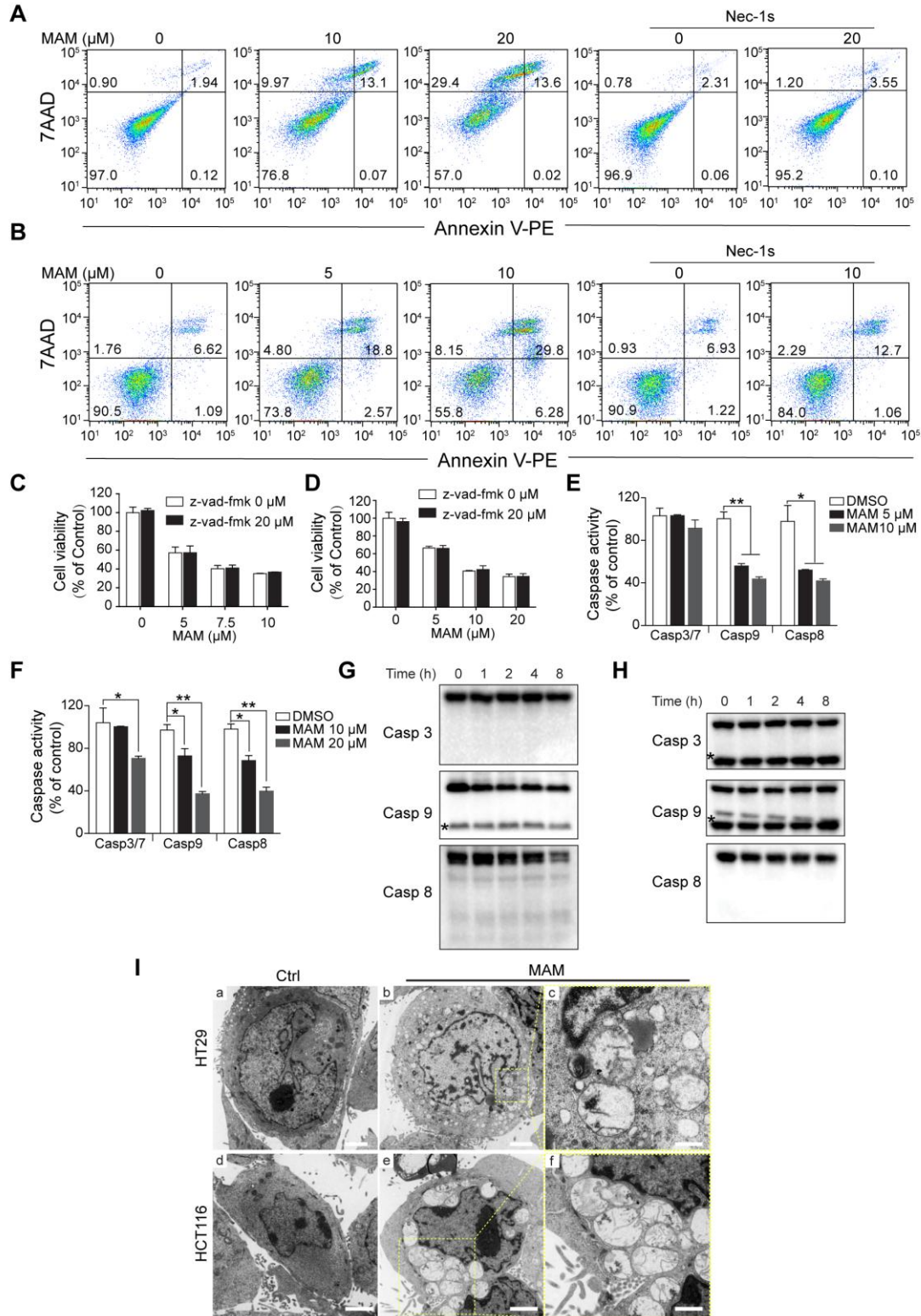
Fig. 2. MAM-induced non-apoptotic cell death in colon cancer cells. HT29 (A) and HCT116

(B) cells were treated with different concentrations of MAM for 6 h in the presence or

absence of Nec-1s (50 and 20 μM, respectively) pretreatment for 1 h. The apoptosis was

detected with Annexin V-PE/7AAD double staining by flow cytometry. Effect of pan-caspase inhibitor z-vad-fmk on MAM-induced HCT116 (C) and HT29 (D) cell death. Cells were treated with z-vad-fmk (20 μM) for 2 h, followed by MAM treatment for another 8 h. Cell viability was measured by MTS assay. Error bars represent standard deviations of three separate experiments. (E and F) Caspase activities were determined using Caspase-Glo Assay Kit after MAM treatment on HCT116 (E) and HT29 (F) cells. *$P < 0.05$; **$P < 0.01$, analyzed by one-way ANOVA with Dunnett's *post hoc* test. (G and H) The expression levels of caspase 3, 8, and 9 in the MAM-treated HCT116 (G) and HT29 (H) cells (10 and 20 μM, respectively) were determined by Western blot analysis. *, non-specific bands. (I) TEM analysis of MAM-treated HCT116 and HT29 cells for 8 hours (10 and 20 μM, respectively). a and d, control cells; b and e, swollen mitochondria; c and f, high-power magnifications showing swollen and damaged mitochondria. Scale bars: 2 μm (a, b, d and e); 0.5 μm (c); 1 μm (f). Results are representative of at least three individual experiments.

MAM induced RIP1/RIP3-mediated necroptosis

The effect of Nec-1s on MAM-induced ATP levels was examined to confirm the involvement of necroptosis in MAM-induced cell death. Nec-1s pretreatment significantly reversed the ATP decline induced by MAM treatment (Fig. 3A, B). A necrosis inhibitor IM-54 was also used to exclude the involvement of unregulated necrosis [24]. IM-54 (10 μM) co-treatment did not influence the cytotoxicity of MAM towards HCT116 and HT29 cells (Fig. 3C, D). The initiation of necroptosis requires RIP1 and RIP3 [25]. RIP1 and RIP3 could induce autophosphorylation on serine

residue 166 (Ser166) and serine residue 227 (Ser227), respectively [5]. Phosphorylated RIP3 targets the phosphorylation of MLKL at the T357 and S358 and thus compromises plasma membrane integrity [5]. Therefore, the phosphorylation of RIP1, RIP3, and MLKL is considered a hallmark of necroptosis [26]. The expression and phosphorylation of these proteins were detected to verify the occurrence of necroptosis. The phosphorylation levels of RIP1 (Ser166) and RIP3 (S227) were up-regulated after MAM treatment was administered. The phosphorylation of RIP1 was sustained, whereas the phosphorylation of RIP3 began to decrease at 8 h (Fig. 3E). The formation of RIP1/RIP3-containing necrosome complex was confirmed through necrosome immunoprecipitation by using RIP3 antibody [27]. Interestingly, RIP3 immunoprecipitation following MAM treatment revealed its interaction with RIP1, which was weakened by Nec-1s (Fig. 3F). The phosphorylation of MLKL was only observed in MAM-treated HT29 cells. We then detect whether these observations correlate with cell death. The knockdown of RIP1 and RIP3 expression in HCT116 cells partially reversed the viability of MAM-exposed cells, whereas the knockdown of MLKL did not elicit any effect (Fig. 3G, for siRNA effects, see Supplementary Fig. S1). The MLKL inhibitor necrosulfonamide (NSA), which targets Cys86 of MLKL [28], also did not influence MAM-induced colon cancer cell death (Fig. 3H). Similar effects were observed in HT29 cells.

Therefore, the pharmacological and genetic suppression of RIP1 and RIP3, not MLKL, could attenuate MAM-induced cytotoxicity. These data indicated that MAM induced RIP1/RIP3 necrosome formation and initiated necroptosis without affecting

MLKL.
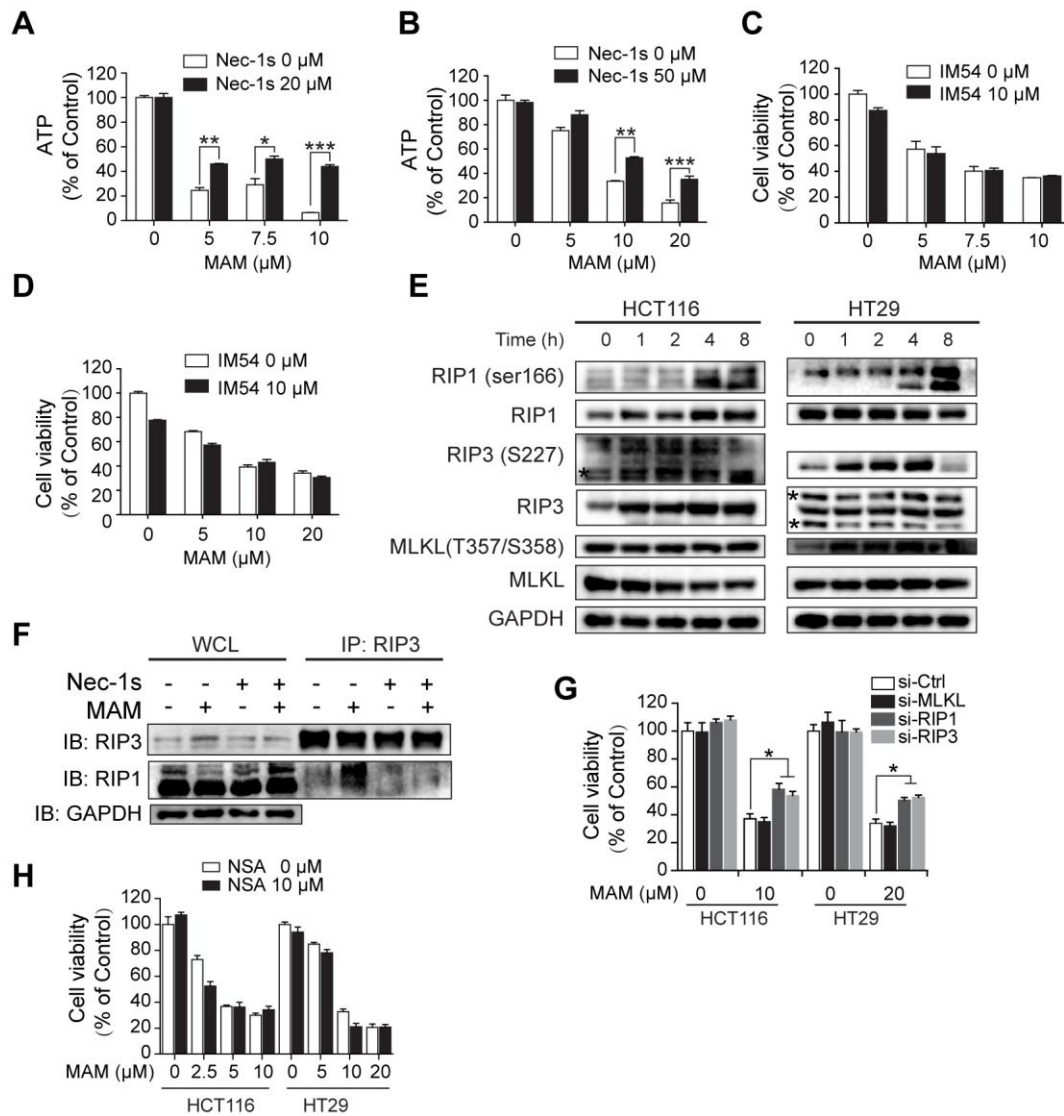
Fig. 3. MAM-induced RIP1/RIP3 dependent necroptosis in colon cancer cells. (A and B) The MTS assay evaluating the effect of necroptosis inhibitor Nec-1s on MAM-induced HCT116 (A) and HT29 (B) cell death. Cells were treated with different concentrations of MAM for 8 h in the presence or absence of Nec-1s pretreatment for 1 h. Error bars represent standard deviations of three separate experiments. *$P < 0.05$; **$P < 0.01$; ***$P < 0.001$, analyzed by two-way ANOVA with Bonferroni *post hoc* test. (C and D) The MTS assay evaluating the effect of IM54 on MAM-induced HCT116 (C) and HT29 (D) cell death. Cells were treated

with different concentrations of MAM for 8 h with or without IM54 (10 μM) pretreatment for

1 h. (E) Immunoblots evaluating the expression of phosphorylated RIP1 (Ser166),

RIP3(S227), MLKL(T357/S358) and corresponding total forms protein expression in MAM

-treated HCT116 and HT29 cells (10 μM and 20 μM, respectively). GAPDH is used as a

loading control. (F) RIP1/RIP3 complex formation by immunoprecipitation using RIP3

antibody from MAM-treated HCT116 cells for 8 h. Immunoblots determining the RIP3 and

RIP1 expression in whole-cell lysates (WCL) and immunoprecipitates are included. (G)

Effects of RIP1, RIP3, or MLKL knockdown on necroptosis. HCT116 and HT29 cells were

transfected with siRNAs and then treated with MAM for 8 h. Cell viabilities were evaluated

by MTS assay. Error bars represent standard deviations of three separate experiments. $*P <$

0.05, analyzed by one-way ANOVA with Dunnett's *post hoc* test. (H) Effects of NSA on

necroptosis. Cells were treated with different concentrations of MAM for 8 h in the presence

or absence of NSA (10 μM) pretreatment for 1 h. Error bars represent standard deviations of

three separate experiments.

MAM induces mitochondrial ROS generation and loss of MMP

Necrosomes have been reported to impair mitochondria energy metabolism by

disturbing ROS homeostasis, leading to ATP depletion, mitochondrial depolarization,

and eventually cell death [3]. Thus, the cascade of events followed by the necrosome

complex formation was studied. The mitochondrial ROS production was evaluated by

flow cytometry using MitoSOX Red staining. As shown in Fig. 4A, the fluorescence

intensity increased in a time-dependent manner in MAM-treated HCT116 and HT29

cells (10 and 20 μM, respectively). This was later confirmed by the reactivation of both cytosolic (c-) and mitochondrial (m-) aconitase, which is one of the most sensitive target for superoxide [29] (Supplementary Fig. S2). Remarkably, MAM-induced mitochondrial ROS generation in both cell lines was attenuated by Nec-1s (Fig. 4B, Supplementary Fig. S2). This finding suggested that the RIP1/RIP3 necrosome complex played a critical role in regulating mitochondrial ROS generation.

To determine the site of MAM-induced intracellular ROS production, HCT116 and HT29 cells were first incubated with either rotenone (Rot), an inhibitor of complex I, TTFA, an inhibitor of Q-binding site of complex II, or antimycin A (AA), an inhibitor of Qi-binding site of complex III. In both cell lines MAM treatment resulted in a 3- to 4- fold increases in MitoSox Red intensity when compared to control group (Fig. 4C). Among the three electron transport chain blockers, only TTFA decreased MAM-induced fluorescence intensity nearly to the basal level. AA treatment alone resulted in an increased fluorescence intensity in both cell lines. In addition, MAM combined with AA treatment resulted in a 5- and 9- fold increases in fluorescence intensity in HCT116 and HT29 cells, respectively. Similar effects were observed in Rot-treated groups. These results suggested complex II as the source of mitochondrial ROS.

As pharmacological inhibitors are not exactly specific to the expected cellular target, we also performed experiments using molecular techniques. Overexpression of mitochondrial antioxidant protein MnSOD completely prevented the cytotoxicity effect of MAM when compared with the vector transfected cells (Fig. 4D).

Furthermore, MnSOD overexpression, as well as TTFA pretreatment, notably protected against cell death upon treatment with MAM (Fig. 4E). Conversely, Rot and AA pretreatment resulted in a slightly decrease of cell viability when compared to MAM alone treated cells. Taken together, these results showed the crucial role of mitochondrial superoxide in MAM induced oxidative stress and cell death.

The effect of MAM on MMP was assessed by time-lapse imaging with TMRM (Supplementary Video 1). TMRM is a cell-permeant dye that accumulates in active mitochondria with intact membrane potentials. Upon loss of MMP, TMRM ceases accumulation and thus reduces fluorescence. TMRM levels decreased at an early time point after HCT116 cells were incubated with MAM (10 μM) and then almost disappeared after 6 h of treatment. Notably, MAM-induced loss of MMP was dramatically reversed by Nec-1s pretreatment (Fig. 4F), indicating that loss of MMP is one of the downstream execution pathways of RIP1/RIP3 containing necrosome. The mitochondrial permeability transition (MPT) pore has been reported to be involved in several forms of cell death [3]. The MPT pore component cyclophilin D plays an important role in necrotic cell death [30,31]. However, cyclosporine A (CsA), a cyclophilin D inhibitor, pretreatment showed no protective effect either on MAM-induced mitochondrial depolarization (Supplementary Fig. S3A) or cell death (Supplementary Fig. S3B). Taken together, these results showed that MAM induced mitochondrial ROS generation and CsA-independent MMP loss.
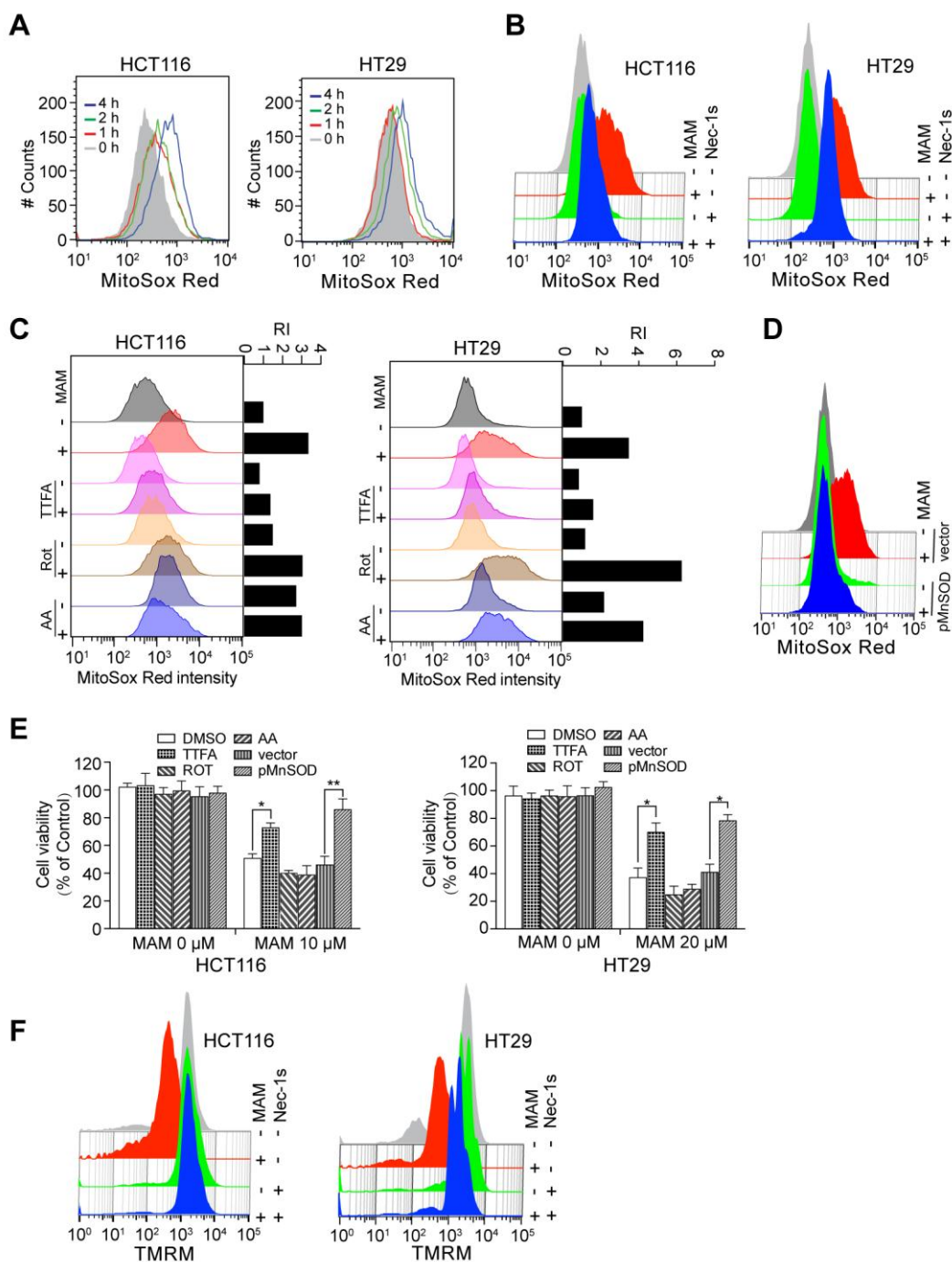
Fig. 4. Effect of Nec-1s and electron transport chain inhibitors on MAM-mediated mitochondrial dysfunction. (A) Time response analysis of MAM treatment on mitochondrial ROS generation. HCT116 and HT29 cells were treated with MAM (10 and 20 μM, respectively) for the indicated time periods and then stained with MitoSox Red (5 μM) and analyzed by flow cytometry. (B) Effect of Nec-1s on MAM-induced mitochondrial ROS

generation. HCT116 and HT29 cells were treated with MAM (10 and 20 μM, respectively) for 4 h in the presence or absence of Nec-1s (20 and 50 μM, respectively) pretreatment for 1 h, followed by MitoSox staining and flow cytometry analysis. (C) Effects of different electron transport chain inhibitors on MAM-induced mitochondrial ROS generation. HCT116 and HT29 cells were treated with MAM (10 and 20 μM, respectively) for 4 h in the presence or absence of electron transport chain inhibitors (20 μM TTFA, 10 μM AA, 5 μM Rot) pretreatment for 1 h, followed by MitoSox staining and flow cytometry analysis. (D) Effects of overexpression of MnSOD or empty vector on MAM induced mitochondrial ROS generation by flow cytometry analysis. HCT116 cells were transfected with vector encoding human MnSOD or control empty vector (as described before), followed by MAM treatment for 4 h. Then cells were stained with MitoSox Red (5 μM) and analyzed by flow cytometry. (E)Effects of different electron transport chain inhibitors or overexpression of MnSOD on MAM-induced cell death by MTS assay. HCT116 and HT29 cells were either pretreated with electron transport chain inhibitors (20 μM TTFA, 10 μM AA, 5 μM Rot) for 1 h or transfected with vector encoding human MnSOD or empty vector, followed by MAM (10 and 20 μM, respectively) treatment for 8 h. MTS assay was used to evaluate cell viability. Error bars represent standard deviations of three separate experiments. $*P < 0.05$; $**P < 0.01$, analyzed by one-way ANOVA with Dunnett's *post hoc* test. (F) Effect of Nec-1s on MAM-induced loss of MMP. HCT116 and HT29 cells were treated as described in (B), followed by TMRM staining and flow cytometry analysis.

Cytosolic calcium accumulation and JNK activation is essential for cell death

Next, the molecular link between RIP1/RIP3 necrosome and MMP with mitochondrial ROS imbalance was explored. Calcium has long been regarded as an important cell death modulator [32]. Increased cytoplasmic calcium was reported to trigger necroptosis in several experimental models by activating calcium-calmodulin kinase (CaMK) II, followed by RIP1 phosphorylation and activation [8]. With the fluorescent probe Fluo-3/AM, we measured the intracellular calcium at different time points by flow cytometry. A time-dependent accumulation of calcium was observed in both HCT116 and HT29 cells (Fig. 5A). The elevation of cytosolic calcium was further confirmed by GCaMP3, a genetically encoded calcium indicator [33]. The GCaMP3 fluorescent signal was remarkably increased at 4 h after MAM treatment in both HCT116 and HT29 cells (Supplementary Fig. S4). Inconsistent with the previous report that cytosolic calcium functions at upstream of RIP1 activation [8], MAM-induced calcium accumulation could be largely attenuated by RIP1 inhibitor Nec-1s, which was comparable to that of BAPTA-AM, a permeable calcium chelator (Fig. 5B). Furthermore, BAPTA-AM (1 μM) could confer protection against MAM-induced cytotoxicity (Fig. 5C).

Considering that extracellular Ca^{2+} influx is a major mechanism of increased intracellular Ca^{2+} [34], we further examined MAM-triggered calcium accumulation. On the basis of the data in Supplementary Fig. S5A, we selected 1 mM ethyleneglycoltetraacetic acid (EGTA), a Ca^{2+} chelating agent. EGTA pretreatment did

not protect HCT116 cells from MAM-induced cell death (Fig. 5D). This finding indicated that cytosolic calcium accumulation was caused by Ca^{2+} released from stored intracellular Ca^{2+} and not attributed to Ca^{2+} influx from the extracellular environment. Parallel experiments were conducted using HT29 cells, and similar results were obtained (Supplementary Fig. S5B).
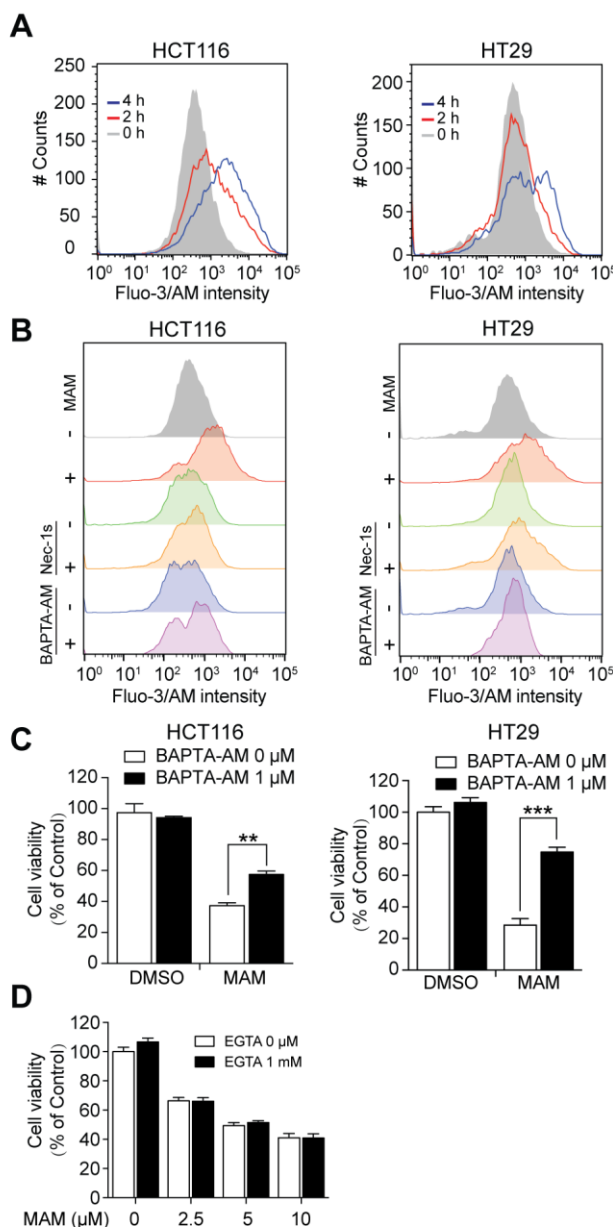
Fig. 5. Cytosolic calcium is an essential mediator for necroptosis. (A) Time response analysis of MAM on calcium concentrations indicated with Fluo-3/AM fluorescence intensity by flow

cytometry. HCT116 and HT29 cells were treated with MAM (10 and 20 μM, respectively) for 2 or 4 h, followed by Fluo-3/AM staining and flow cytometry. (B) Effect of necroptosis inhibitor Nec-1s and calcium chelator BAPTA-AM on MAM-induced calcium elevation. HCT116 and HT29 cells were treated with MAM (10 and 20 μM, respectively) for 4 h in the presence or absence of Nec-1s (20 and 50 μM, respectively) or BAPTA (1 μM) pretreatment for 1 h and then stained with Fluo-3/AM before flow cytometry analysis. (B) Protective effect of BAPTA-AM on necroptosis. HCT116 and HT29 cells were pretreated with BAPTA (1 μM) for 1 h and then challenged with MAM (10 and 20 μM, respectively) for another 8 h. Cell viability was determined by MTS assay. Error bars represent standard deviations of three separate experiments. **$P < 0.01$; ***$P < 0.001$, analyzed by two-way ANOVA with Bonferroni *post hoc* test. (D) Extracellular calcium influx is not involved in necroptosis. HCT116 cells were treated with MAM for 8 h with or without EGTA (1 μM) pretreatment for 2 h. Cell viability was measured by MTS assay.

We previously reported the important role of JNK activation in MAM-induced cell death in several cell lines [22]. Here, the phosphorylation of JNK in MAM-treated HCT116 and HT29 cells was detected as well (Fig. 6A). Similarly, a rapid JNK activation was observed after MAM treatment for 1 h in both cell lines. This increase of JNK phosphorylation was sustained for at least 4 h. To explore whether calcium accumulation might be responsible for JNK activation, we pre-chelated the cytosolic calcium with BAPTA-AM (1 μM) for 1 h and then treated with MAM for another 2 h. Both calcium chelator BAPTA-AM and RIP1 inhibitor Nec-1s could suppress MAM-induced JNK phosphorylation to the basal level, comparable to the SP600125

pretreated group (Fig. 6B). This suggests that RIP1 phosphorylation and calcium accumulation resulted in sustained JNK activation. Furthermore, both JNK inhibitor SP600125 and JNK knockdown significantly reversed MAM-induced cell death, implying the essential role of JNK activation in MAM-induced necroptosis (Fig. 6C, D, for siRNA knockdown efficiencies, Supplementary Fig. S6). It's also worth to mention that JNK activation occurred faster than the RIP1 phosphorylation. This implies that RIP1/RIP3 complex and calcium are the main but not the only contributors to JNK activation.

To further elucidate the relationship between RIP1/RIP3 complex and calcium accumulation as well as JNK activation, we performed immunoprecipitation with antibody against RIP3. Results showed that neither inhibition of JNK by SP600125 or specific siRNA nor calcium chelation by BAPTA-AM could affect the RIP1/RIP3 complex formation (Fig. 6E). These results support the finding that calcium accumulation and JNK activation function downstream of RIP1/RIP3 complex formation.

A

HCT116   HT29

Time (h)   0 1 2 4 8   0 1 2 4 8

p-JNK2
p-JNK1

JNK2
JNK1

GAPDH

B

MAM   - + - + - + - +

BAPTA-AM   Nec-1s   SP600125

p-JNK2
*
p-JNK1

JNK2
JNK1

GAPDH

C

☐ SP600125 0 μM
■ SP600125 5 μM

Cell viability (% of Control)

DMSO   MAM

*

D

☐ si-Ctrl
■ si-JNK1/2

Cell viability (% of Control)

DMSO   MAM

*

E

WCL   IP: RIP3

si-Ctrl   + + - -   + + - -
si-JNK1/2 - - + +   - - + +
MAM   - + - +   - + - +

IB: RIP3

IB: RIP1

IB: GAPDH

SP600125   BAPTA-AM

MAM   - + - + - +

WCL
IB: RIP1
IB: RIP3
IB: GAPDH

IP: RIP3
IB: RIP1
IB: RIP3
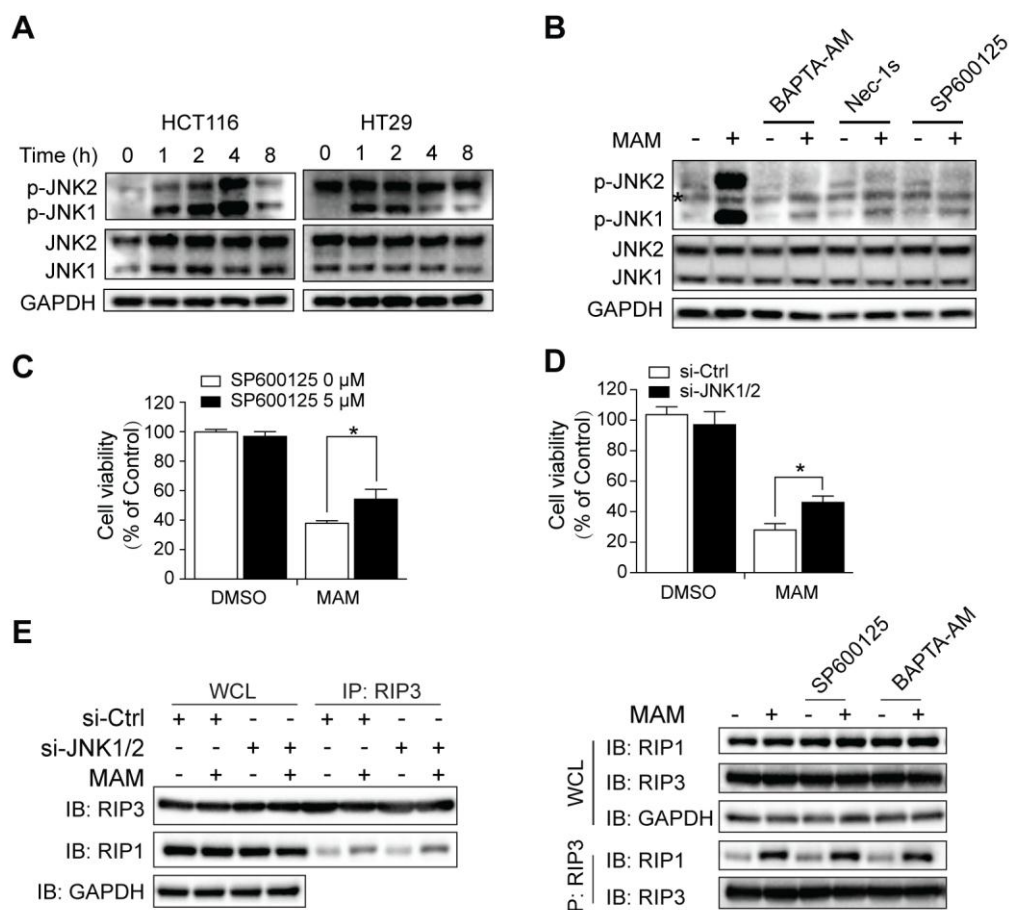
Fig. 6. Sustained JNK activation triggered by calcium in necroptosis. (A) Immunoblots evaluating expression of phosphorylated JNK (p-JNK) and JNK after the MAM treatment in HCT116 (10 μM) and HT29 (20 μM) cells. GAPDH is used as a loading control. (B) Effect of BAPTA-AM, Nec-1s, and SP600125 on JNK activation by western blot analysis. HCT116 cells were pretreated with BAPTA (1 μM), Nec-1s (20 μM), or SP600125 (5 μM) for 1 h and then challenged with MAM (10 μM) for another 4 h. *, non-specific bands. (C) Effect of JNK inhibitor SP600125 on necroptosis. HCT116 cells were treated with MAM for 8 h in the presence or absence of SP600126 (5 μM) pretreatment for 1 h. Cell viabilities were evaluated by MTS assay. Error bars represent standard deviations of three separate experiments. $*P <$ 0.05, analyzed by two-way ANOVA with Bonferroni *post hoc* test. (D) Effect of JNK knockdown on necroptosis. HCT116 and HT29 cells were transfected with siRNAs and then

treated with MAM for 8 h. Cell viabilities were evaluated by MTS assay. Error bars represent standard deviations of three separate experiments. *$P < 0.05$, analyzed by two-way ANOVA with Bonferroni *post hoc* test. (E) Effects of JNK inhibition and calcium chelation on RIP1/RIP3 complex formation by immunoprecipitation using RIP3 antibody from MAM-treated HT29 cells for 8 h. HT29 cells were transfected with siRNAs or pretreated with JNK inhibitor SP600125 or calcium chelator BAPTA-AM for 1 h, followed by MAM treatment for another 8 h. Immunoblots determining the RIP3 and RIP1 expression in whole-cell lysates (WCL) and immunoprecipitates are included.

CaMK II, the downstream effector of calcium signaling, was reported to coordinate calcium-induced necroptosis in human neuroblastoma [8]. It may also be a candidate for JNK activation [35]. MAM induced CaMK II phosphorylation in both HCT116 and HT29 cells in a time-dependent manner (Fig. 7A). However, pretreatment with KN93, the CaMK II inhibitor, showed no effect on JNK activation and MAM-induced cell death in either cell lines (Fig. 7B, C). Thus, CaMK II phosphorylation is increased but not indispensable for MAM-induced necroptosis in colon cancer cells.
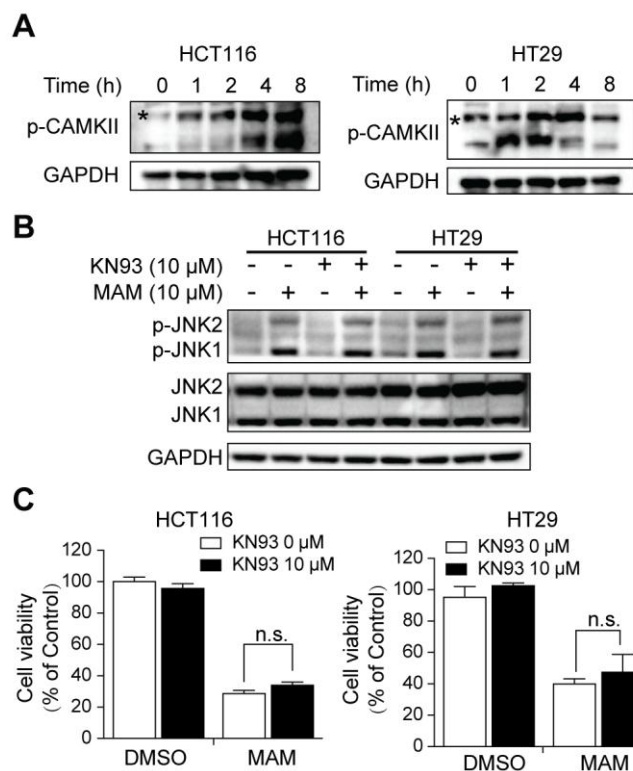
Fig. 7. Dispensable role of CaMKII in necroptosis. (A) Western blot of p-CaMKII protein levels relative to GAPDH in MAM-treated HCT116 and HT29 cells (10 and 20 μM, respectively). *, non-specific bands. (B) Effect of CaMKII inhibitor KN93 on MAM-induced JNK activation by western blot analysis. HCT116 and HT29 cells were treated with MAM (10 and 20 μM, respectively) for 8 h with or without KN93 pretreatment (10 μM) for 1 h. (C) Dispensable role of KN93 on MAM-induced necroptosis. HCT116 cells were pretreated with KN93 (10 μM) for 1 h and then challenged with MAM (10 μM) for another 8 h. Cell viability was measured by MTS assay. Error bars represent standard deviations of three separate experiments. n.s., no significance, analyzed by two-way ANOVA with Bonferroni *post hoc* test.

Inhibition of JNK and chelation of calcium rescues cells from mitochondrial ROS imbalance and depolarization

Considering the essential role of JNK activation and calcium accumulation in MAM-induced necroptosis, we determined whether mitochondrial ROS imbalance and depolarization were mediated by these factors. The suppression of JNK by SP600125 and calcium chelation by BAPTA-AM could significantly protect cells from the elevation of MitoSox Red fluorescence (Fig. 8A). The loss of TMRM fluorescence was also blocked by either SP600125 or BAPTA-AM pretreatment (Fig. 8B). These results suggested that calcium accumulation and JNK activation might function as the upstream mechanisms of mitochondrial dysfunction.
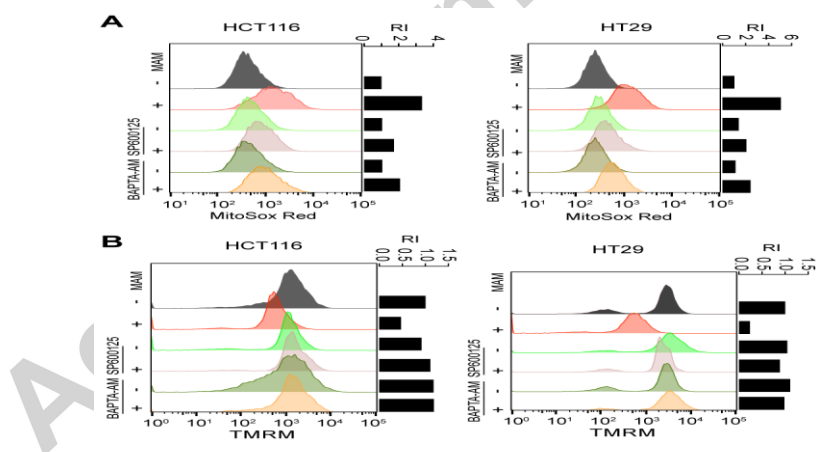
Fig. 8. JNK and calcium regulate the mitochondrial dysfunction. (A) Effects of SP600125 and BAPTA-AM on MAM-induced mitochondrial ROS generation. HCT116 and HT29 cells were treated with MAM for 4 h with or without SP600125 (5 μM) and BAPTA-AM (1 μM) pretreatment for 1 h and then stained with MitoSox Red before flow cytometry analysis. Data are expressed in terms of relative intensity (RI) compared with control group. (B) Effect of

SP600125 and BAPTA-AM on MAM-induced loss of MMP. HCT116 and HT29 cells were treated as described in (A), and then stained with TMRM before flow cytometry analysis. Data are expressed in terms of relative intensity compared with control group.

TNFα and LMP was not involved in MAM-induced necroptosis

Tumor necrosis factor-α (TNFα) has been demonstrated to trigger necroptosis in a number of cell types [36-39]. Autocrine production of TNFα was required for natural compound-induced necroptosis [40]. We then detected whether autocrine production of TNFα is involved in MAM-induced necroptotic cell death. The TNFα levels maintained at low basal levels in both cell lines even after MAM treatment for 8 h (below the minimum detection limit, data now shown), excluding the contribution of TNFα in this process.

The connection between Ca^{2+} homeostasis and lysosomal membrane permeabilization (LMP) has been reported by the observation that TNF induced a slight increase of intracellular calcium level resulting in enlarged lysosomes that were prone to LMP [41]. LMP causes leakage of the lysosomal proteases, namely cathepsins, into the cytosol, which could initiate necroptosis [42]. To further elucidate the mechanisms underlying MAM-induced cell death, its effects on lysosomes was studied. For this purpose, different methods were used to assess LMP. First, Lysotracker red, which accumulates inside acidic organelles (lysosomes and late endosomes), was used to monitor the lysosomes. No increase of Lysotracker red fluorescence was detected in MAM-treated HCT116 cells during 4 h, whereas a slight decrease was observed in MAM-treated HT29 cells (Supplementary Fig. S7A).

Considering that weakened Lysotracker fluorescence may reflect LMP and/or an increase in lysosomal pH [42], the researchers used acridine orange (AO), a lysosomotropic metachromatic fluorochrome, to check lysosomal alterations. AO-stained cells exhibit weakened red fluorescence and strengthened blue fluorescence after LMP [43]. Similar to that of Lysotracker red staining, no significant alterations in red or blue fluorescence were observed in MAM-treated HCT116 cells, indicating that LMP might not be involved in this process (Supplementary Fig. S7B). To further exclude the role of LMP, cytotoxicity studies were carried out with cathepsin inhibitors. Pepstatin A inhibited aspartic proteinases, mainly cathepsins D and E [44]. E64D could rapidly inhibit the activities of the cysteine proteinases such as cathepsins B, H, and L [45]. Cathepsin Inhibitor 1 is an inhibitor of cathepsin L, L2, S, K, and B [46]. However, none of these inhibitors conferred protection of cells from MAM-induced cell death (Supplementary Fig. S7C). Therefore, LMP was not involved in MAM-induced necroptosis.

MAM induces necroptosis in a p53-independent manner

p53 has recently been reported to execute necroptosis by inducing cathepsin Q that cooperates with ROS [47]. Cytotoxicity tests were performed with HCT116 $p53^{+/+}$ and HCT116 $p53^{-/-}$ cells to explore the potential role of p53 in MAM-induced necroptosis. Similar IC_{50} were obtained in HCT116 $p53^{+/+}$ and HCT116 $p53^{-/-}$ cells (Supplementary Fig. S8). Therefore, MAM induced necroptosis in a p53-independent manner.

Discussion

As an inducible, alternative form of programmed cell death, necroptosis has attracted significant attention. It offers promising novel strategies for anti-cancer therapy, especially for reversing drug resistance [48,49]. However, few natural compounds that can trigger necroptosis exist, and even less is known about the detailed molecular signaling pathways. For example, shikonin was proposed to circumvent cancer drug resistance through induction of necroptosis [11,50]. Neoalbaconol-induced necroptosis mediated by RIP1/NF-κB-dependent expression of TNFα and RIPK3-dependent generation of ROS [40]. However, the detailed molecular pathways that crosslink RIP1 or RIP3 with the final cell demise remain to be clarified. As RIP1 has important roles in both cell survival and cell death [51] and could positively or negatively regulate necroptosis [52,53], detection of its total protein expression as necroptotic biomarker was unconvincing. Instead, the phosphorylation status should be evaluated simultaneously.

We previously reported the necroptotic and apoptotic effects of MAM on A549, MCF7, and B16-F10 cells [22]. In the present study, MAM was identified as a necroptosis inducer in human colon cancer cells. Cell cytotoxicity demonstrated significant decrease in ATP levels (Fig. 1). Annexin V-7AAD double-staining assay revealed no evident early apoptotic feature, which is consistent with the observation that caspase 3, 8, and 9 were not cleaved and the broad-spectrum caspase inhibitor z-VAD-fmk did not elicit protective effects (Fig. 2A, B, C, G, H). Caspase activities

decreased in both cell lines, and this finding further indicated that compromised caspase activities, especially caspase 8, facilitated necroptosis (Fig. 2D, E) [54,55]. The involvement of necroptosis was further confirmed by detecting RIP1/RIP3 complex formation and RIP1 and RIP3 phosphorylation (Fig. 3E, F). Moreover, both pharmacological inhibition of RIP1 by small molecule Nec-1s and genetic suppression of RIP1 and RIP3 by corresponding si-RNA could partially reverse MAM-induced cytotoxicities. Therefore, RIP1 and RIP3 played essential roles in mediating MAM-induced necroptosis.

Either calcium overload or JNK activation is involved in the conditioning and execution of necroptosis [25,56]. Robust and sustained JNK activation induced by hydrogen peroxide has been reported in MAM-induced cell death in A549, MCF7, and B16-F10 cells in our previous study [22]. In this study, early and prolonged JNK activation was also observed, which was triggered by the elevated Ca^{2+}. This finding was confirmed by genetically encoded GcAMP 3 calcium indicator by confocal microscope and Fluo-3 AM staining by flow cytometry. Furthermore, both inhibition of JNK activation by SP600125 and calcium accumulation by calcium chelator BAPTA-AM confer protections against MAM-induced mitochondrial ROS elevation, loss of MMP, and the final ATP depletion. To the best of our knowledge, this is the first report to show the interaction between JNK activation and calcium elevation in mediating necroptosis. The failure of EGTA to protect cells from MAM-induced cell death revealed that the increase in calcium levels was caused by the release of stored intracellular Ca^{2+} and not by the influx of extracellular Ca^{2+}. However, the release of

Ca^{2+} from the endoplasmic reticulum, the main organelle for Ca^{2+} storage [57], should be further clarified.

ROS production has been reported to be executioner and mediator of necroptosis [58, 59]. In this context, complex II inhibitor TTFA attenuated MAM induced mitochondrial ROS generation and cell death, indicating the important role of complex II in ROS induction and mitochondrial dysfunction. The protective effect of overexpression of MnSOD further confirmed the role of mitochondria in ROS production and cell death. Blocking electron transport chain using compounds such as AA and Rot has long been reported to increase mitochondrial ROS production [60]. The observation that complex I inhibitor Rot and complex III inhibitor AA increased MAM induced ROS generation accompanied by slightly enhanced cytotoxicity of MAM further proofed the mitochondrial ROS deleterious. A better understanding of how mitochondrial complex II modulates ROS generation and cell death would offer new perspectives to interfere with necroptosis under pathophysiological conditions.

CaMKII functions as a RIP3 substrate in ischemia- and oxidative-induced myocardial necroptosis [61]. This substrate is responsible for RIP1 phosphorylation in human neuroblastoma cells [8]. In our study, the inability of KN93 to promote MAM-induced JNK activation and cell death precludes the involvement of CaMKII phosphorylation in MAM-induced necroptosis, although CaMKII phosphorylation levels increased in a time-dependent manner.

MLKL phosphorylation triggers its oligomerization and membrane localization and consequently causes membrane rupture [4-6], which has been recognized as an

important biomarker and final executor of necroptosis *in vitro*. MLKL was phosphorylated at T357/S358 in MAM-treated HT29 cells but not in HCT116 cells. However, NSA, which targets Cys86 of MLKL to inhibit its membrane translocation [5,28], and si-RNA-mediated knockdown of MLKL failed to protect MAM-induced cell death. These results suggested that the membrane was ruptured in a MLKL-independent manner. Although NSA attenuates neoalbaconol-induced cell death [40], its role in natural compound-induced necroptosis has yet to be determined and fully elucidated [11-13,50]. Calcium influx mediated by MLKL has been considered a major mechanism of plasma membrane rupture during necroptosis [4]. However, our study demonstrated that the increase in intracellular calcium levels was not caused by the influx of extracellular calcium, and the chelation of extracellular Ca^{2+} with EGTA showed no protective effect against MAM-induced cell death. These findings suggested that a MLKL-independent Ca^{2+} increase in the process of necroptosis might occur.

TNF signaling pathway exemplifies the induction of necroptosis [3]. Autocrine TNFα has also been reported to be involved in natural-compound-induced necroptosis [40]. However, no autocrine TNFα was detected in this study. The involvement of other triggers, such as CD95L and TNF-related apoptosis-inducing ligand [38], in the upstream of RIP1/RIP3 necrosome formation should be further classified. High intracellular Ca^{2+} levels could facilitate LMP, leading to the release of hydrolytic enzymes, especially cathepsins, which are detrimental to cells [3]. LMP can function as the cause or consequence of regulated necrosis [3] and can act as a mediator of

natural compound-induced necroptosis [62]. However, MAM did not affect LMP, and cathepsins failed to prevent cell death. Thus, LMP was not included in our study. p53 has been proposed to regulate MPT-mediated necrosis [63,64], but the precise mechanism remains unclear [65]. In our study, neither MPT nor p53 dependence was detected.

In summary, MAM was identified as a necroptosis trigger in human colon cancer cells (Fig. 9). Necroptotic signaling is dependent on RIP1/RIP3 complex formation, followed by calcium accumulation and subsequently resulted in JNK activation. Increased calcium levels and sustained JNK activation induced mitochondrial dysfunction and caused cell death. MAM-induced necroptosis was independent of TNFα, p53, MLKL, and LMP. These results provided new insights into the molecular regulation of necroptosis in human colon cancer cells.
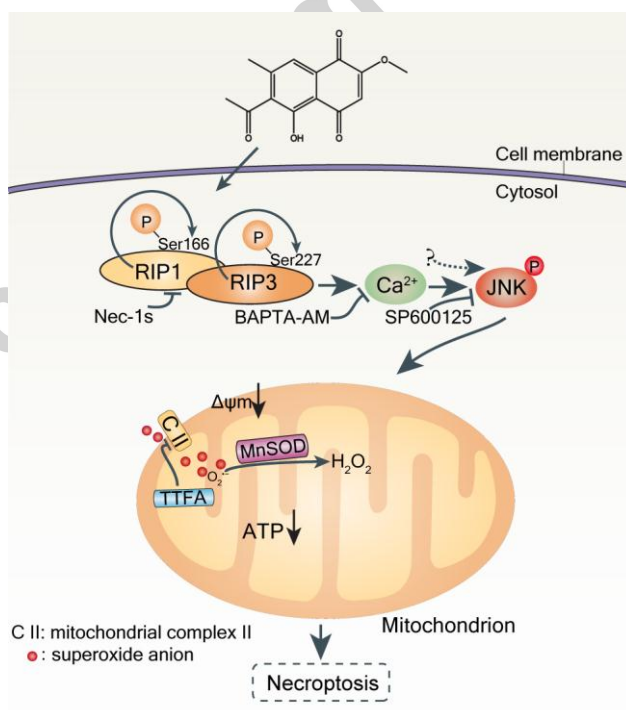
Fig. 9. Schematic representation of necroptotic signaling stimulated by MAM in human colon cancer cells. MAM induces autophosphorylation of RIP1 and RIP3 at ser166 and ser227,

respectively, leading to RIP1/RIP3 necrosome formation. Then, RIP1/RIP3 necrosome caused calcium accumulation, followed by JNK activation, which could also be activated by other unknown pathways. As the downstream effects of JNK activation, mitochondrial dysfunction is induced which consists of deleterious ROS generation derived from mitochondrial complex II, loss of MMP, and ATP depletion.

Conflict of interest

The authors declare no conflict of interest.

Acknowledgments

References

[1] A. Linkermann, D.R. Green, Necroptosis, N. Engl. J. Med. 370 (5) (2014) 455-465.

[2] A. Degterev, Z. Huang, M. Boyce, Y. Li, P. Jagtap, N. Mizushima, G.D. Cuny, T.J.

Mitchison, M.A. Moskowitz, J. Yuan, Chemical inhibitor of nonapoptotic cell death with therapeutic potential for ischemic brain injury, Nat. Chem. Biol. 1 (2) (2005) 112-119.

[3] T. Vanden Berghe, A. Linkermann, S. Jouan-Lanhouet, H. Walczak, P. Vandenabeele, Regulated necrosis: the expanding network of non-apoptotic cell death pathways, Nat. Rev. Mol. Cell Biol. 15 (2) (2014) 135-147.

[4] Z. Cai, S. Jitkaew, J. Zhao, H.C. Chiang, S. Choksi, J. Liu, Y. Ward, L.G. Wu, Z.G. Liu, Plasma membrane translocation of trimerized MLKL protein is required for TNF-induced necroptosis, Nat. Cell Biol. 16 (1) (2014) 55-65.

[5] H. Wang, L. Sun, L. Su, J. Rizo, L. Liu, L.F. Wang, F.S. Wang, X. Wang, Mixed lineage kinase domain-like protein MLKL causes necrotic membrane disruption upon phosphorylation by RIP3, Mol. Cell 54 (1) (2014) 133-146.

[6] X. Chen, W. Li, J. Ren, D. Huang, W.-t. He, Y. Song, C. Yang, W. Li, X. Zheng, P. Chen, Translocation of mixed lineage kinase domain-like protein to plasma membrane leads to necrotic cell death, Cell Res. 24 (1) (2014) 105-121.

[7] D.E. Clapham, Calcium signaling, Cell 131 (6) (2007) 1047-1058.

[8] M. Nomura, A. Ueno, K. Saga, M. Fukuzawa, Y. Kaneda, Accumulation of cytosolic calcium induces necroptotic cell death in human neuroblastoma, Cancer Res. 74 (4) (2014) 1056-1066.

[9] D. Hanahan, R.A. Weinberg, The hallmarks of cancer, Cell 100 (1) (2000) 57-70.

[10] D. Hanahan, R.A. Weinberg, Hallmarks of cancer: the next generation, Cell 144 (5) (2011) 646-674.

[11] W. Han, L. Li, S. Qiu, Q. Lu, Q. Pan, Y. Gu, J. Luo, X. Hu, Shikonin circumvents cancer drug resistance by induction of a necroptotic death, Mol. Cancer Ther. 6 (5) (2007) 1641-1649.

[12] Z. Fu, B. Deng, Y. Liao, L. Shan, F. Yin, Z. Wang, H. Zeng, D. Zuo, Y. Hua, Z. Cai, The anti-tumor effect of shikonin on osteosarcoma by inducing RIP1 and RIP3 dependent necroptosis, BMC Cancer 13 (2013) 580.

[13] C.J. Huang, Y.A. Luo, J.W. Zhao, F.W. Yang, H.W. Zhao, W.H. Fan, P.F. Ge, Shikonin Kills Glioma Cells through Necroptosis Mediated by RIP-1, Plos One 8 (6) (2013).

[14] Y. Kimura, M. Kozawa, K. Baba, K. Hata, New constituents of roots of Polygonum cuspidatum, Planta Med. 48 (3) (1983) 164-168.

[15] H.W. Rauwald, H. Miething, 2-Methoxystypandrone, a new naphthoquinone from Rhamnus fallax B, Z. Naturforsch., C: Biosci. 38C(1-2) (1983) 17-20.

[16] A.B. Hughes, M.V. Sargent, Synthesis of 2-methoxystypandrone: comments on the structure of ventilaginone, Journal of the Chemical Society, Perkin Transactions 1 (3) (1989) 449-452.

[17] S.B. Singh, P.L. Graham, R.A. Reamer, M.G. Cordingley, Discovery, total synthesis, HRV 3C-protease inhibitory activity, and structure-activity relationships of 2-methoxystypandrone and its analogues, Bioorg Med. Chem. Lett. 11 (24) (2001) 3143-6.

[18] W.F. Chiou, J.F. Liao, C.Y. Huang, C.C. Chen, 2-Methoxystypandrone represses RANKL-mediated osteoclastogenesis by down-regulating formation of

TRAF6-TAK1 signalling complexes, Br. J. Pharmacol. 161 (2) (2010) 321-335.

[19] Y.B. Li, Z.Q. Lin, Z.J. Zhang, M.W. Wang, H. Zhang, Q.W. Zhang, S.M. Lee, Y.T. Wang, P.M. Hoi, Protective, antioxidative and antiapoptotic effects of 2-methoxy-6-acetyl-7-methyljuglone from Polygonum cuspidatum in PC12 cells, Planta Med. 77 (4) (2011) 354-361.

[20] C.M. Chern, Y.H. Wang, K.T. Liou, Y.C. Hou, C.C. Chen, Y.C. Shen, 2-Methoxystypandrone ameliorates brain function through preserving BBB integrity and promoting neurogenesis in mice with acute ischemic stroke, Biochem. Pharmacol. 87 (3) (2013) 502-514.

[21] S. Kuang, C. Qi, J. Liu, X. Sun, Q. Zhang, Z. Sima, J. Liu, W. Li, Q. Yu, 2-Methoxystypandrone inhibits STAT3 and NF-kappaB Signaling by inhibiting Janus kinase 2 and IkappaB kinase, Cancer Sci. 105 (4) (2014) 473-480.

[22] W. Sun, J.L. Bao, W. Lin, H.W. Gao, W.W. Zhao, Q.W. Zhang, C.H. Leung, D.L. Ma, J.J. Lu, X.P. Chen, 2-Methoxy-6-acetyl-7-methyljuglone (MAM), a natural naphthoquinone, induces NO-dependent apoptosis and necroptosis by H_2O_2-dependent JNK activation in cancer cells, Free Radic. Biol. Med. 92 (2016) 61-77.

[23] J. Wesiersk-Gadek, J. Wojciechowski, CellTiter-Glo Assay: application for assessing direct cytotoxicity and for determining cell proliferation and cell cycle regulation, Cell Notes 6 (2003) 251-306.

[24] K. Dodo, M. Katoh, T. Shimizu, M. Takahashi, M. Sodeoka, Inhibition of hydrogen peroxide-induced necrotic cell death with 3-amino-2-indolylmaleimide

derivatives, Bioorg. Med. Chem. Lett. 15 (12) (2005) 3114-3118.

[25] P. Vandenabeele, L. Galluzzi, T. Vanden Berghe, G. Kroemer, Molecular mechanisms of necroptosis: an ordered cellular explosion, Nat. Rev. Mol. Cell Biol. 11 (10) (2010) 700-714.

[26] S. He, S. Huang, Z. Shen, Biomarkers for the detection of necroptosis, Cell. Mol. Life Sci. 73 (11-12) (2016) 2177-2181.

[27] A. Degterev, W. Zhou, J.L. Maki, J. Yuan, Assays for necroptosis and activity of RIP kinases, Methods Enzymol. 545 (2014) 1-33.

[28] L. Sun, H. Wang, Z. Wang, S. He, S. Chen, D. Liao, L. Wang, J. Yan, W. Liu, X. Lei, X. Wang, Mixed lineage kinase domain-like protein mediates necrosis signaling downstream of RIP3 kinase, Cell 148 (1-2) (2012) 213-27.

[29] P.R. Gardner, D. Nguyen, C.W. White, Aconitase is a sensitive and critical target of oxygen poisoning in cultured mammalian cells and in rat lungs, Proc. Natl. Acad. Sci. USA 91(25) (1994) 12248-12252.

[30] C.P. Baines, R.A. Kaiser, N.H. Purcell, N.S. Blair, H. Osinska, M.A. Hambleton, E.W. Brunskill, M.R. Sayen, R.A. Gottlieb, G.W. Dorn, Loss of cyclophilin D reveals a critical role for mitochondrial permeability transition in cell death, Nature 434 (7033) (2005) 658-662.

[31] T. Nakagawa, S. Shimizu, T. Watanabe, O. Yamaguchi, K. Otsu, H. Yamagata, H. Inohara, T. Kubo, Y. Tsujimoto, Cyclophilin D-dependent mitochondrial permeability transition regulates some necrotic but not apoptotic cell death, Nature 434 (7033) (2005) 652-658.

[32] S. Orrenius, V. Gogvadze, B. Zhivotovsky, Calcium and mitochondria in the regulation of cell death, Biochem. Biophys. Res. Commun. 460 (1) (2015) 72-81.

[33] L. Tian, S.A. Hires, T. Mao, D. Huber, M.E. Chiappe, S.H. Chalasani, L. Petreanu, J. Akerboom, S.A. McKinney, E.R. Schreiter, C.I. Bargmann, V. Jayaraman, K. Svoboda, L.L. Looger, Imaging neural activity in worms, flies and mice with improved GCaMP calcium indicators, Nat. Methods 6 (12) (2009) 875-81.

[34] M.D. Bootman, T.J. Collins, C.M. Peppiatt, L.S. Prothero, L. MacKenzie, P. De Smet, M. Travers, S.C. Tovey, J.T. Seo, M.J. Berridge, Calcium signalling—an overview, Semin. Cell Dev. Biol. 12 (1) (2001) 3-10.

[35] C.Y. Wu, H.L. Hsieh, C.C. Sun, C.M. Yang, IL- 1β induces MMP- 9 expression via a $Ca2^+$- dependent CaMKII/JNK/c- JUN cascade in rat brain astrocytes, Glia 57 (16) (2009) 1775-1789.

[36] D. Vercammen, P. Vandenabeele, R. Beyaert, W. Declercq, W. Fiers, Tumour necrosis factor-induced necrosis versus anti-Fas-induced apoptosis in L929 cells, Cytokine 9 (11) (1997) 801-808.

[37] S. He, L. Wang, L. Miao, T. Wang, F. Du, L. Zhao, X. Wang, Receptor interacting protein kinase-3 determines cellular necrotic response to TNF-α, Cell 137 (6) (2009) 1100-1111.

[38] N. Holler, R. Zaru, O. Micheau, M. Thome, A. Attinger, S. Valitutti, J.-L. Bodmer, P. Schneider, B. Seed, J. Tschopp, Fas triggers an alternative, caspase-8–independent cell death pathway using the kinase RIP as effector molecule, Nat.

Immunol. 1 (6) (2000) 489-495.

[39] Y. Lin, S. Choksi, H.-M. Shen, Q.-F. Yang, G.M. Hur, Y.S. Kim, J.H. Tran, S.A. Nedospasov, Z.-g. Liu, Tumor necrosis factor-induced nonapoptotic cell death requires receptor-interacting protein-mediated cellular reactive oxygen species accumulation, J. Biol. Chem. 279 (11) (2004) 10822-10828.

[40] X. Yu, Q. Deng, W. Li, L. Xiao, X. Luo, X. Liu, L. Yang, S. Peng, Z. Ding, T. Feng, Neoalbaconol induces cell death through necroptosis by regulating RIPK-dependent autocrine TNFα and ROS production, Oncotarget 6 (4) (2015) 1995.

[41] K. Ono, S.O. Kim, J. Han, Susceptibility of lysosomes to rupture is a determinant for plasma membrane disruption in tumor necrosis factor alpha-induced cell death, Mol. Cell. Biol. 23 (2) (2003) 665-676.

[42] P. Boya, G. Kroemer, Lysosomal membrane permeabilization in cell death, Oncogene 27 (50) (2008) 6434-6451.

[43] A. Terman, T. Kurz, Lysosomal iron, iron chelation, and cell death, Antioxid. Redox Signal. 18 (8) (2013) 888-898.

[44] S. Seelmeier, H. Schmidt, V. Turk, K. Von Der Helm, Human immunodeficiency virus has an aspartic-type protease that can be inhibited by pepstatin A, Proc. Natl. Acad. Sci. USA 85 (18) (1988) 6612-6616.

[45] A.J. Barrett, A. Kembhavi, M. Brown, H. Kirschke, C. Knight, M. Tamai, K. Hanada, L-trans-Epoxysuccinyl-leucylamido (4-guanidino) butane (E-64) and its analogues as inhibitors of cysteine proteinases including cathepsins B, H and L,

Biochem. J. 201 (1) (1982) 189-198.

[46] N. Asaad, P.A. Bethel, M.D. Coulson, J.E. Dawson, S.J. Ford, S. Gerhardt, M. Grist, G.A. Hamlin, M.J. James, E.V. Jones, Dipeptidyl nitrile inhibitors of Cathepsin L, Bioorg. Med. Chem. Lett. 19 (15) (2009) 4280-4283.

[47] H.-C. Tu, D. Ren, G.X. Wang, D.Y. Chen, T.D. Westergard, H. Kim, S. Sasagawa, J.J.-D. Hsieh, E.H.-Y. Cheng, The p53-cathepsin axis cooperates with ROS to activate programmed necrotic death upon DNA damage, Proc. Natl. Acad. Sci. USA 106 (4) (2009) 1093-1098.

[48] S. Fulda, Therapeutic exploitation of necroptosis for cancer therapy, Semin. Cell Dev. Biol. 35 (2014) 51-56.

[49] W. Zhou, J. Yuan, Necroptosis in health and diseases, Semin. Cell Dev. Biol. 35 (2014) 14-23.

[50] Y. Xuan, X. Hu, Naturally-occurring shikonin analogues – A class of necroptotic inducers that circumvent cancer drug resistance, Cancer Lett. 274 (2) (2009) 233-242.

[51] D.E. Christofferson, Y. Li, J. Yuan, Control of life-or-death decisions by RIP1 kinase, Annu. Rev. Physiol. 76 (2014) 129-50.

[52] S. Orozco, N. Yatim, M.R. Werner, H. Tran, S.Y. Gunja, S.W. Tait, M.L. Albert, D.R. Green, A. Oberst, RIPK1 both positively and negatively regulates RIPK3 oligomerization and necroptosis, Cell Death Differ. 21(10) (2014) 1511-21.

[53] C.J. Kearney, S.P. Cullen, D. Clancy, S.J. Martin, RIPK1 can function as an inhibitor rather than an initiator of RIPK3-dependent necroptosis, FEBS J. 281(21)

(2014) 4921-4934.

[54] Y. Lin, A. Devin, Y. Rodriguez, Z.-g. Liu, Cleavage of the death domain kinase RIP by caspase-8 prompts TNF-induced apoptosis, Genes Dev. 13 (19) (1999) 2514-2526.

[55] S. Feng, Y. Yang, Y. Mei, L. Ma, D.-e. Zhu, N. Hoti, M. Castanares, M. Wu, Cleavage of RIP3 inactivates its caspase-independent apoptosis pathway by removal of kinase domain, Cell. Signal. 19 (10) (2007) 2056-2067.

[56] N. Vanlangenakker, T. Vanden Berghe, P. Vandenabeele, Many stimuli pull the necrotic trigger, an overview, Cell Death Differ. 19 (1) (2012) 75-86.

[57] G.L. Koch, The endoplasmic reticulum and calcium storage, Bioessays 12 (11) (1990) 527-531.

[58] Fulda S, Regulation of necroptosis signaling and cell death by reactive oxygen species, Biol. Chem. 397 (7) (2016) 657-660.

[59] D. E. Christofferson, J. Y. Yuan, Necroptosis as an alternative form of programmed cell death, Curr. Opin. Cell Biol. 22 (2) (2010) 263-268.

[60] M.A. Fath, A.R. Diers, N. Aykin-Burns, A.L. Simons, L. Hua, D.R. Spitz, Mitochondrial electron transport chain blockers enhance 2-deoxy-D-glucose induced oxidative stress and cell killing in human colon carcinoma cells, Cancer Biol. Ther. 8 (13) (2009) 1228-1236.

[61] T. Zhang, Y. Zhang, M. Cui, L. Jin, Y. Wang, F. Lv, Y. Liu, W. Zheng, H. Shang, J. Zhang, CaMKII is a RIP3 substrate mediating ischemia-and oxidative stress-induced myocardial necroptosis, Nat. Med. 22 (2) (2016) 175-182.

[62] Y.M. Ma, Y.M. Peng, Q.H. Zhu, A.H. Gao, B. Chao, Q.J. He, J. Li, Y.H. Hu, Y.B. Zhou, Novel CHOP activator LGH00168 induces necroptosis in A549 human lung cancer cells via ROS-mediated ER stress and NF-κB inhibition, Acta Pharmacol. Sin. 37 (10) (2016) 1381-1390.

[63] A.V. Vaseva, N.D. Marchenko, K. Ji, S.E. Tsirka, S. Holzmann, U.M. Moll, p53 opens the mitochondrial permeability transition pore to trigger necrosis, Cell 149 (7) (2012) 1536-1548.

[64] K. Baumann, Cell death: multitasking p53 promotes necrosis, Nat. Rev. Mol. Cell Biol. 13 (8) (2012) 480-481.

[65] J. Karch, J.D. Molkentin, Is p53 the Long-Sought Molecular Trigger for Cyclophilin D–Regulated Mitochondrial Permeability Transition Pore Formation and Necrosis?, Circ. Res. 111 (10) (2012) 1258-1260.

Graphical abstract
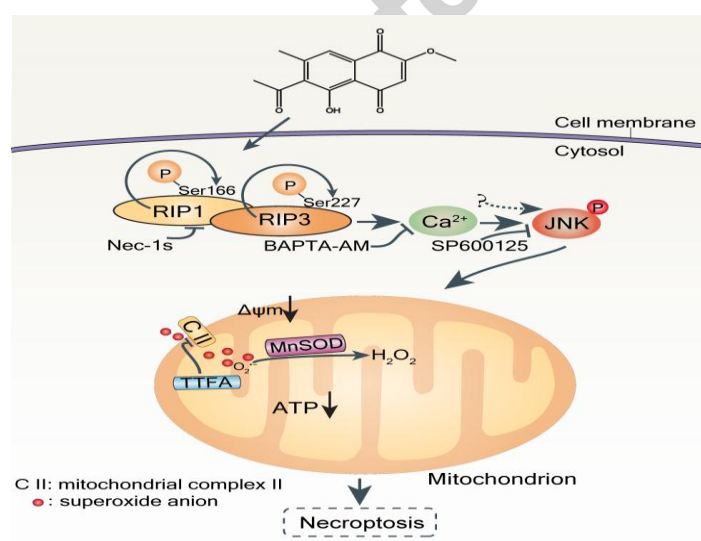
Highlights

- MAM, a natural naphthoquinone, induces RIP1/RIP3 complex dependent necroptosis in human colon cancer cells.

- Calcium accumulation and JNK activation function downstream of RIP1/RIP3 necrosome formation.

- Mitochondrial ROS originated from complex II is playing an essential role in mediating MAM induced necroptosis.

SUPPLEMENTARY FIGURES

Supplementary Video 1. Morphological analysis of cell death induced by MAM on HCT116 cells. HCT116 cells were treated with MAM (10 μM), and then monitored by live-cell imaging in four different channels: differential interface contrast (DIC), the mitochondrial potential probe TMRM (red), the cell impermeable DNA dye SYTOX Green (green), and the cell permeable DNA marker Hoechst 33258 (blue), in a humidified atmosphere containing 5% CO2 at 37°C. Cells were monitored every 15 min for 8 h. Time is indicated as hours:minutes after the addition of MAM. Results are representative of at least three independent experiments. Scale bar: 25 μm.

Supplementary Figure S1. Knockdown efficiencies of siRNA for RIP1, RIP3, and MLKL

on protein expression by western blot analysis after 48 h. GAPDH is used as a loading control.

*, non-specific bands.
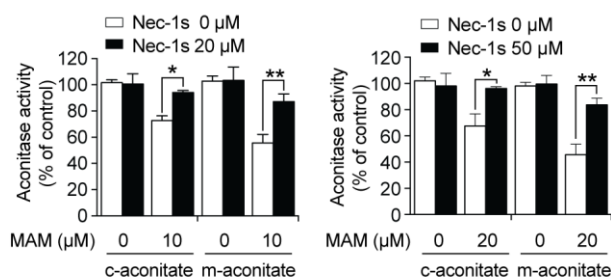
Supplementary Figure S2. Reactivation of aconitase activity by Nec-1s in HCT116 and

HT29 cells. HCT116 and HT29 cells were treated with MAM (10 and 20 μM, respectively)

for 4 h in the absence or presence of Nec-1s pretreatment (20 and 50 μM, respectively) for 1 h.

Aconitase activity was measured according to the manufacturer's instructions. Error bars

represent standard deviations of three separate experiments. *$P < 0.05$; **$P < 0.01$, analyzed

by two-way ANOVA with Bonferroni *post hoc* test.
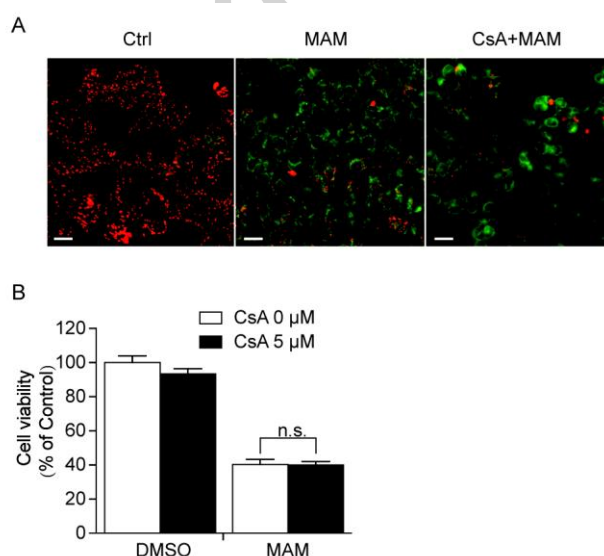
Supplementary Figure S3. CsA-dependent MPT is not involved in necroptosis. (**A**) Effect of

CsA on mitochondrial membrane potential. HCT116 cells were treated with or without CsA

(5 μM) for 1 h and then challenged with MAM for another 4 h. Images were captured by IN

Cell Analyzer 2000 after JC-1 staining (2 μg/mL, 30 min, 37 °C). Scale bar: 10 μm. (**B**) MTS

assay evaluating effect of CsA on cell death. HCT116 cells were treated with MAM (10 μM)

for 8 h in the presence or absence of CsA (5 μM) pretreatment for 1 h. Error bars represent

standard deviations of three separate experiments. n.s., no significance, analyzed by two-way

ANOVA with Bonferroni *post hoc* test.
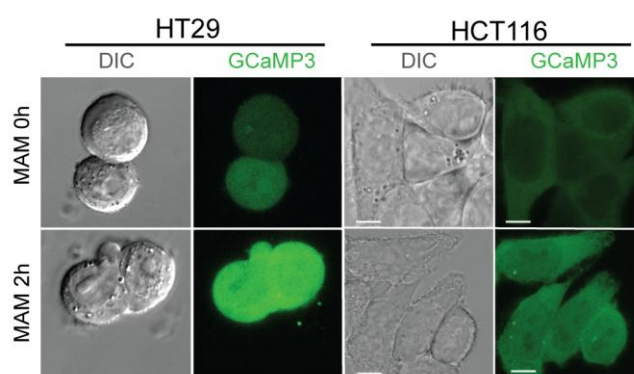
Supplementary Figure S4. Detection of calcium with encoded calcium indicator GCaMP3.

HCT116 and HT29 cells were transfected with GCaMP3 plasmid for 24 h, followed by MAM

(10 and 20 μM, respectively) or vehicle control (DMSO) treatment for 4 h. Images were

captured by a confocal microscope. Scale bar: 5 μm.
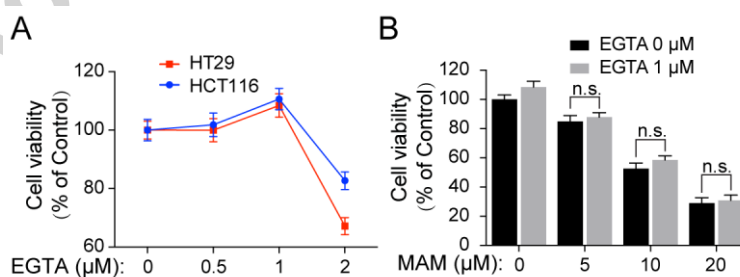
Supplementary Figure S5. Extracellular calcium influx is not involved in necroptosis. (**A**)

MTS assay evaluating the cytotoxicity of EGTA. HCT116 and HT29 cells were treated with

different concentrations of EGTA for 8 h. (**B**) Effect of EGTA on necroptosis. HT29 cells

were treated with MAM for 8 h in the presence or absence of EGTA (1 mM) pretreatment for

1 h. MTS assay was used to test the cell viability. Error bars represent standard deviations of

three separate experiments. n.s., no significance, analyzed by two-way ANOVA with

Bonferroni *post hoc* test.
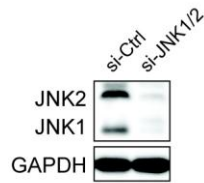
Supplementary Figure S6. Knockdown efficiency of siJNK on protein level by western blot

analysis. HCT116 cells were transfected with si-JNK or si-Ctrl (scrambled siRNA) for 48 h.

GAPDH is used as a loading control.
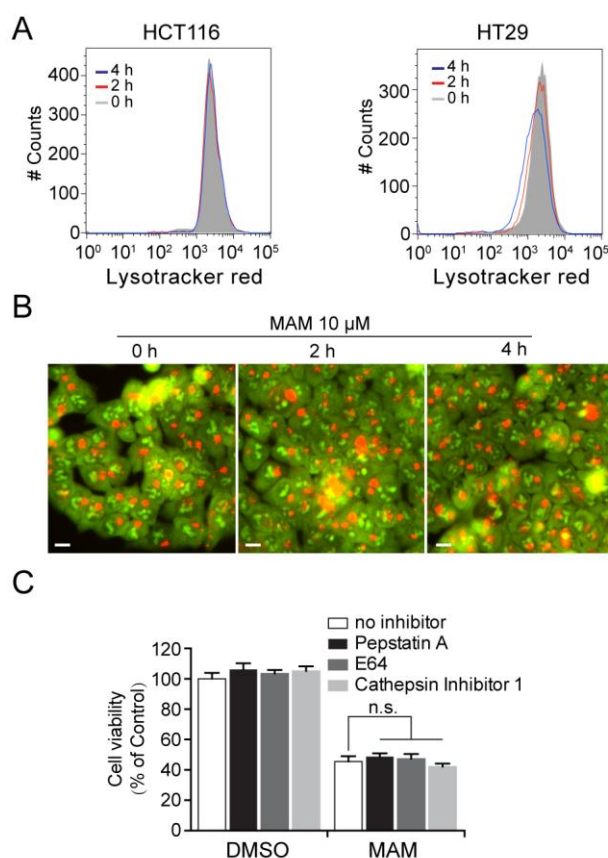
Supplementary Figure S7. LMP is not involved in necroptosis. (**A**) Time response analysis of MAM treatment on Lysotracker Red staining intensity. HCT116 or HT29 cells were treated with MAM for the indicated time periods, and then stained with Lysotracker Red for 1 h, followed by flow cytometry analysis. (**B**) LMP evaluation by AO staining. HCT116 cells were treated with MAM (10 μM) for the indicated time periods and then stained with AO, followed by image capture using IN Cell Analyzer 2000. Scale bar: 10 μm. (**C**) Effects of various cathepsin inhibitors on MAM-induced cell death. HCT116 cells were pretreated for 2 h with various inhibitors (Pepstatin A, 50 μM; E64, 50 μM; Cathepsin Inhibitor 1, 80 μM) or vehicle control (DMSO), followed by addition of MAM (10 μM) for another 8 h. Error bars represent standard deviations of three separate experiments. n.s., no significance, analyzed by one-way ANOVA with Dunnett's *post hoc* test.
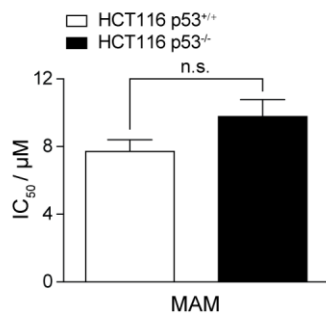
Supplementary Figure S8. MAM-induced necroptosis is in a p53-independent manner. IC_{50} values of MAM against HCT116 p53$^{+/+}$ and HCT116 p53$^{-/-}$ cells after 8 h incubation. n.s., no significance, analyzed by Student's *t* test.